Received: 5 September 2018 | Revised: 9 October 2019 | Accepted: 10 October 2019

DOI: 10.1002/glia.23739

GLIA

WILEY

RESEARCH ARTICLE

Inhibition of inflammatory cells delays retinal degeneration in experimental retinal vein occlusion in mice

Joël Jovanovic[1,2] | Xuan Liu[1,3] | Despina Kokona[1,2] | Martin S. Zinkernagel[1,2] | Andreas Ebneter[1,2]

[1]Department of Ophthalmology, Inselspital, Bern University Hospital and University of Bern, Bern, Switzerland

[2]Department for BioMedical Research, University of Bern, Bern, Switzerland

[3]Department of Ophthalmology, 1st Affiliated Hospital of Xi'an Jiaotong University, Xi'an Shaanxi, China

Correspondence
Andreas Ebneter, Department of Ophthalmology, Inselspital, Bern University Hospital and University of Bern, Bern, Switzerland.
Email: andreas.ebneter@insel.ch

Funding information
Chinese Scholarship Council, Grant/Award Number: 201600160105; Swiss Government Excellence Scholarship, Grant/Award Number: 2017.0620; Dr. Streuli-Fonds; Prix Retina 2016 grant; CTU Research-Grant, Grant/Award Number: 84800858

Abstract

The role of microglia in retinal inflammation is still ambiguous. Branch retinal vein occlusion initiates an inflammatory response whereby resident microglia cells are activated. They trigger infiltration of neutrophils that exacerbate blood–retina barrier damage, regulate postischemic inflammation and irreversible loss of neuroretina. Suppression of microglia-mediated inflammation might bear potential for mitigating functional impairment after retinal vein occlusion (RVO). To test this hypothesis, we depleted microglia by PLX5622 (a selective tyrosine kinase inhibitor that targets the colony-stimulating factor-1 receptor) in fractalkine receptor reporter mice (*Cx3cr1*$^{gfp/+}$) subjected to various regimens of PLX5622 treatment and experimental RVO. Effectiveness of microglia suppression and retinal outcomes including retinal thickness as well as ganglion cell survival were compared to a control group of mice with experimental vein occlusion only. PLX5622 caused dramatic suppression of microglia. Despite vein occlusion, reappearance of green fluorescent protein positive cells was strongly impeded with continuous PLX5622 treatment and significantly delayed after its cessation. In depleted mice, retinal proinflammatory cytokine signaling was diminished and retinal ganglion cell survival improved by almost 50% compared to non-depleted animals 3 weeks after vein occlusion. Optical coherence tomography suggested delayed retinal degeneration in depleted mice. In summary, findings indicate that suppression of cells bearing the colony-stimulating factor-1 receptor, mainly microglia and monocytes, mitigates ischemic damage and salvages retinal ganglion cells. Blood–retina barrier breakdown seems central in the disease mechanism, and complex interactions between different cell types composing the blood–retina barrier as well as sustained hypoxia might explain why the protective effect was only partial.

KEYWORDS

blood–retina barrier, inflammation, ischemia, microglia, receptor tyrosine kinase inhibitor, retinal ganglion cell, retinal vein occlusion

Joël Jovanovic and Xuan Liu have equally contributed to this study.

1 | INTRODUCTION

Retinal vein occlusion (RVO) is a frequent cause of vision loss in elderly populations and has a prevalence of up to 2% among individuals over 40 years of age (Klein, Klein, Moss, & Meuer, 2000). The pathogenesis is believed to involve atherosclerotic changes within the vessel walls, leading to stasis, thrombosis, and occlusion of veins. There are two distinct types of RVO: branch retinal vein occlusion (BRVO) and central retinal vein occlusion (CRVO). Both types can be nonischemic or ischemic, the latter having a worse prognosis in terms of vision and potential complications. Both forms may lead to atrophy of the inner retinal layers, mainly affecting ganglion cells (RGCs) and the retinal nerve fiber layer (Kim, Shin, Lee, Jo, & Kim, 2014; Rogers et al., 2010). In patients with RVO, increased expression of inflammatory proteins in the vitreous has been described (Ehlken et al., 2015). Microglia have been recognized as key mediators of neuroinflammation in the brain and the retina, and have been shown to produce cytokines such as tumor necrosis factor alpha (TNF-α) which can induce neuronal apoptosis (Guadagno, Xu, Karajgikar, Brown, & Cregan, 2013). Neuroinflammation is a common feature of many acute neurological events such as stroke (Wang, Tang, & Yenari, 2007) or spinal cord injury (Fleming et al., 2006). A laser-induced experimental BRVO (eBRVO) model has previously been established in mice (Ebneter, Agca, Dysli, & Zinkernagel, 2015; Zhang et al., 2007) that closely mimics the pathology, including increased vascular endothelial growth factor (VEGF) expression. Previous reports have shown, that eBRVO causes hypoxia in the inner retina, activation of resting retinal microglia, and recruitment of blood derived monocytes into the area of hypoxia (Ebneter, Kokona, Schneider, & Zinkernagel, 2017). However, the influence and consequences of neuroinflammation on RGC survival after an ischemic insult have so far not been thoroughly investigated.

Myeloid cells, including microglia cells or macrophages and osteoclasts, specifically express colony-stimulating factor-1 receptor (CSF1R) on their surface (S. Patel & Player, 2009). In the healthy central nervous system (CNS), the CSF1R is only expressed on microglial cells (Erblich, Zhu, Etgen, Dobrenis, & Pollard, 2011; Nandi et al., 2012). Its ligands, CSF1 and IL-34, regulate proliferation, differentiation, and survival of these cells (Gomez-Nicola, Fransen, Suzzi, & Perry, 2013; Hume & MacDonald, 2012; S. Patel & Player, 2009). Furthermore, it has been shown that mice lacking either CSF1 or CSF1R have a diminished macrophage/microglia population in different tissues (Erblich et al., 2011; Ginhoux et al., 2010). Recently, potent orally administered selective CSF1R inhibitors have become available. These compounds inhibit the intracellular tyrosine kinase domain of the CSF1R and c-Kit which results in suppression of CNS microglia in adult mice (Elmore et al., 2014), depleting up to 99% of microglia after 7 days (Spangenberg et al., 2016). This effect is reversible, with complete recovery of microglia numbers after drug cessation. Recently, an even more selective molecule (PLX5622, Plexxikon Inc., Berkeley, CA) that has no or negligible inhibitory effects on c-Kit (Dagher et al., 2015; Dharmarajan, Fisk, Sorenson, Sheibani, & Belecky-Adams, 2017) has been developed. This compound allows selective depletion of CNS microglia in adult mice without affecting other cell populations nor having relevant side effects in terms of inflammation or behavioral changes (Dharmarajan et al., 2017; Elmore et al., 2014). Previously, we have shown that PLX5622 permeates the blood–retina barrier very well and significantly depletes retinal microglia (Ebneter, Kokona, Jovanovic, & Zinkernagel, 2017). In this study, we combined the eBRVO model with retinal microglia depletion to evaluate whether microglia influence RGC survival in eBRVO.

2 | MATERIALS AND METHODS

2.1 | Animals

Heterozygous mice selectively expressing green fluorescent protein (GFP) in microglia under the control of the *Cx3cr1* gene were obtained by crossbreeding wild type Balb/cAnNCrl females with male transgenic homozygous fractalkine receptor reporter mice ($Cx3cr1^{gfp/gfp}$) on a balb/c background (Jung et al., 2000). In such mice, homing and infiltration should not be significantly different from wild type mice (Kezic, Xu, Chinnery, Murphy, & McMenamin, 2008). For all experiments, mice were sex- and age-matched (between 6 and 8 weeks of age). Mice were maintained in a temperature and humidity-controlled animal facility in individually ventilated cages on a 12-hr light–dark schedule. All animals had access to food and water ad libitum. This study was approved by the local Animal Ethics Committee (Veterinärdienst des Kantons Bern: BE 14/16) and conformed to the Association for Research in Vision an Ophthalmology Statement for the Use of Animals in Ophthalmic and Vision Research.

2.2 | PLX5622 administration

Six- to eight-week-old heterozygous mice were fed with chow containing PLX5622 (1,200 parts per million [ppm] formulated in AIN-76A standard rodent diet; Research Diets Inc., New Brunswick, NJ) or identical chow without drug for control animals.

2.3 | Anesthesia

Anesthesia was used for in vivo imaging and experimental laser induction of eBRVO. Animals received an intraperitoneal injection of medetomidine (1 mg/kg, Dormitor 1 mg/ml, Provet AG, Lyssach, Switzerland) and ketamine (80 mg/kg, Ketalar 50 mg/ml, Parke-Davis, Zurich, Switzerland). At the end of investigational procedures, but earliest after 30 min, medetomidine was antagonized with atipamezole (2.3 mg/kg, Antisedan 5 mg/ml, Provet AG).

2.4 | In vivo fundus autofluorescence imaging

To visualize PLX5622-induced depletion and recovery of retinal GFP^+ microglia/macrophages longitudinally, retinas of anesthetized animals were imaged with confocal scanning laser ophthalmoscopy (SLO, Heidelberg Spectralis HRA + OCT; Heidelberg Engineering GmbH,

Heidelberg, Germany). Images were acquired in the blue light (488 nm) fundus autofluorescence mode using a noncontact ultra-widefield 102° lens (Heidelberg Engineering GmbH). Mydriasis was induced by tropicamide 0.5%/phenylephrine 2.5% eyedrops (Hospital Pharmacy, Inselspital, Bern, Switzerland). Hydroxypropylmethylcellulose 20 mg/ml (Methocel 2%; OmniVision AG, Neuhausen, Switzerland) was applied on the eyes to avoid corneal surface drying out due to loss of blink reflex during anesthesia. Acquired images were exported as jpeg for further analysis.

2.5 | Monitoring of retinal microglia depletion

Kinetics of retinal microglia depletion was assessed by confocal SLO in nine sex- and age-matched (2 months of age) heterozygous *Cx3cr1*$^{gfp/+}$ reporter mice. All animals were imaged at the start of the experiment to establish a mean baseline microglia count before commencement of continuous PLX6522 treatment for 3 weeks. Four time points were defined for follow-up in vivo imaging: 24 hr after onset of PLX5622 administration and then weekly at 7, 14, and 21 days. After de-identification, all acquired images were transferred and processed in the ImageJ software (Version 1.51j8, National Institutes of Health) for semi-automated cell counting. In short, pictures were converted into 8-bit images and background subtraction was applied with a rolling ball radius of 20 pixels. Images were then smoothed before the "Find maxima" function was used (with the *preview point selection* option turned on) to count microglia cells. Noise tolerance was adjusted manually by the grader (JJ) in an iterative process to ascertain appropriate identification of cells to be included in the count.

2.6 | BRVO model and experimental groups

In each eye, venous supply to about half of the retina was blocked by targeting two to three major veins about two disc diameters superior and nasal to the optic disc as previously described in Ebneter et al. (2015). The inferotemporal half of the retina was considered non-occluded. Briefly, after intravenous injection of 0.15 ml rose Bengal (5 mg/ml saline; Sigma-Aldrich Switzerland, Buchs, Switzerland) into the tail vein, eBRVO was induced by laser (532 nm) photocoagulation (Visulas 532s; Carl Zeiss Meditec AG, Oberkochen, Germany) with a slit lamp adapter (Iridex Corporation, Mountain View, CA) mounted on a commercial slit lamp (BM900; Haag-Streit AG, Koeniz, Switzerland). To visualize blood vessel occlusion during laser treatment, a 2-mm fundus laser lens for mice (Ocular Instruments, Inc., Bellevue, WA) was used. Hydroxypropylmethylcellulose 2% was used as viscous coupling fluid between lens and cornea. The laser was set to 50 μm spot size, 160 mW laser intensity, and exposure time was 0.8 s. Up to three burns were necessary to achieve complete occlusion of the vessels. Stasis of blood flow distal to the occlusion site was directly observed by the investigator to confirm successful eBRVO.

Three different eBRVO groups were defined. Two groups were pretreated with PLX5622 for 2 weeks before eBRVO induction, whereas the third group received control food (no PLX5622) throughout the whole experiment. After eBRVO induction, one of the PLX5622 pretreated groups was continuously fed with PLX5622 for the follow-up period of three more weeks while the other was switched to control chow. The groups were designated *BRVO + PLX5622* group (continuous depletion) and *BRVO + Microglia Recovery* group (cessation of depletion after laser), respectively. The control group (*BRVO*) did not get PLX5622 diet at any time.

2.7 | Retinal thickness measurements

Spectral domain optical coherence tomography (Spectralis SD-OCT, Heidelberg Engineering GmbH) was performed to visualize structural and thickness changes of the retina using a 55° lens. SD-OCT volume scans were centered on the optic nerve head and acquired in automatic real-time mode, averaging nine frames per image. Images were exported in XML format to a device-independent retinal layer segmentation software (Orion, Voxeleron LLC., Pleasanton, CA). Total thickness was measured between the inner limiting membrane and Bruch's membrane (Figure S1). Segmentation involved manual correction for all scans (JJ, XL, AE) because the algorithm is currently optimized for human samples. Nevertheless, the editing tool allows efficient segmentation of mouse scans. For subsequent analysis, the software calculated average retinal thickness in all quadrants of a standard Early Treatment Diabetic Retinopathy Study (ETDRS) grid centered at the optic nerve head.

2.8 | Transcardial perfusion fixation and enucleation

At each time point, a minimum of three animals per group were anesthetized for transcardial 0.9% NaCl perfusion, followed by 4% paraformaldehyde solution (PFA, pH 7.4) perfusion for tissue fixation using a peristaltic pump (PLP 380, Dülabo Laborgeräte, Germany). Pentobarbital (Esconarkon, 300 mg/ml, Streuli Pharma AG, Uznach, Switzerland) was diluted with 0.9% NaCl for a 100 mg/ml stock solution. Pentobarbital 150 mg/kg body weight was intraperitoneally injected for terminal anesthesia. After perfusion, right eyes were harvested for whole mount immunohistochemistry and left eyes for paraffin embedding. A conjunctival suture was applied to left eyes before enucleation for orientation during paraffin embedding and sectioning.

2.9 | Retinal whole mount preparation and immunohistochemistry

Right eyes were fixed by immersion in 4% PFA for 10 min followed by removal of cornea and lens under the binocular microscope using surgical micro-scissors. An established staining protocol (Nadal-Nicolas et al., 2009) was followed with slight modifications. In brief, the sclera and choroid were carefully removed before retinas were incubated once more in 4% PFA for 50 min. Fixed retinas were washed four times in 0.5% Triton X-100 phosphate buffer saline (PBS-T) for 10 min. Washed retinas were placed in blocking buffer (5% normal donkey serum [NDS] in 0.2% PBS-T) for 30 min at room temperature on a shaking plate before incubation with a rabbit polyclonal anti-Iba1 antibody (1:250; 016-20001, Wako Chemicals, Osaka, Japan) to

visualize retinal microglia/macrophages and a goat polyclonal anti-Brn3a (C-20) antibody (1:250, Santa Cruz Biotechnology, Dallas, TX) for visualization of retinal ganglion cells, diluted in 1.0% PBS-T and 2% NDS at 4°C for 24 hr on a shaker. Next, retinas were rinsed with 0.5% PBS-T four times for 10 min. The secondary antibodies Alexa Fluor 488 donkey anti-rabbit IgG (A-21206, Invitrogen, Waltham, MA) and Alexa Fluor 593 donkey anti-goat IgG (A-11058, Invitrogen) were diluted 1:250 in 0.5% PBS-T. Retinas were incubated with secondary antibodies for 2 hr at room temperature, followed by three 0.5% PBS-T washes of 15 min each and a final rinse in PBS. To flatten the retinas, four radial cuts were made before whole mounting on glass slides (Menzel SuperFrost, Thermo Fisher Scientific, Waltham, MA) with ganglion cells facing up. Whole mounts were cover-slipped with VECTASHIELD antifade Mounting Medium (Vector Laboratories, Burlingame, CA).

Left eyes were fixed overnight in 4% PFA and then processed for standard paraffin embedding. A microtome (Leica, Biosystems, Muttenz, Switzerland) was used to cut 5 μm thick sections including the optic nerve head. Sections were mounted on glass slides (Menzel SuperFrost) and air-dried. Two nonconsecutive sections of each eye at the level of optic nerve were selected for further processing. For deparaffinization and rehydration, tissue sections were processed in regular xylene and descending ethanol steps. Endogenous peroxidase blocking (30 min in 300 ml methanol + 5.1 ml hydrogen peroxide 30%) was performed followed by PBS washing and antigen retrieval (Tris–EDTA, pH 9) in the microwave for 10 min. Sections were then placed in 5% normal horse serum (NHS) blocking buffer for 30 min. Next, sections were incubated with a rabbit polyclonal anti-Iba1 antibody (1:500 in 5% NHS; 016-20001, Wako Chemicals, Osaka, Japan) overnight at room temperature. After washes with PBS, sections were then incubated for 30 min in biotinylated goat polyclonal anti-rabbit antibody (1:250 in 5% NHS). After another three washes in PBS, slides were finally incubated with HRP-streptavidin-conjugate (1:1000 in 5% NHS; Vector Laboratories) for 60 min at room temperature followed by NovaRED visualization (Vector Laboratories).

2.10 | Microscopy

Whole mounted retinas were scanned with a confocal fluorescence microscope (Fluorescence Olympus BX61VS, Hamburg, Germany) at 10× magnification. Z-stack intervals were 5.5 μm and the scanning depth was adjusted until all layers containing microglia were included. The Olympus VS-ASW software (version 2.9, Olympus Soft Imaging Solutions GmbH, Germany) was used to create a maximum intensity z-projection image for further quantifications. Tissue sections for semiquantitative assessment of $Iba1^+$ cells were directly inspected under the microscope in bright field mode at a magnification of 10×.

2.11 | Semiquantitative assessment of $Iba1^+$ cells on tissue sections

For semiquantitative assessment of $Iba1^+$ cells, two nonconsecutive sections of each eye at the level of optic nerve were selected. An experienced blinded grader (XL) rated the density of $Iba1^+$ cells in occluded and unaffected areas according to templates (Figure 6e; 0 = very low or no $Iba1^+$ cell density; 1 = moderate $Iba1^+$ cell density, 2 = high $Iba1^+$ cell density). The mean rating for each retinal area was then calculated and used for statistical analysis.

2.12 | Quantification of RGC density on retinal whole mounts

Z-projections of retinal whole mount images were quantified using the software ImageJ (Version 1.51j8, National Institutes of Health). Borders between occluded areas and unaffected parts of the retina were traced along major vessels adjacent to occluded veins to separate each retina in parts with ischemia and normal perfusion (Figure S2). The images were converted into 8-bit images and background was subtracted (rolling bar radius: 18 pixel) before a binary mask was created using the same threshold for both areas (occluded vs. nonoccluded). The RGC density for both areas was measured using the "Measure" plugin after defining the borders of the flat mount using the lasso tool. The RGC survival index was calculated by dividing the RGC density in the occluded area by the RGC density in the non-occluded area (Figure S2).

2.13 | Quantitative cytokine expression measurement in the retina

From the literature it is known that several diseases in the CNS, like stroke or BRVO, early induce increased expression of various pro- and anti-inflammatory cytokines that seem related to disease progression (Berti et al., 2002; Clausen et al., 2008; Ebneter, Kokona, Schneider, et al., 2017; Lambertsen, Meldgaard, Ladeby, & Finsen, 2005; Sun, Li, He, Zhang, & Tao, 2013). Activated microglia have been described to be a major source of these early cytokines and seem pivotal for initiation of inflammation and recruitment of circulating inflammatory cells that might be harmful (Chen et al., 2003; Offner et al., 2006) Therefore, two early time points (24 and 72 hr after eBRVO) were selected for retinal cytokine quantification in all experimental groups. For each time point and treatment group, six retinas were pooled for protein extraction and quantification. To determine baseline expression, three healthy naïve mice were additionally assessed. In brief, after cervical dislocation the eyes were immediately enucleated and immersed in ice-cold PBS for whole retina dissection. Retrieved retina was quickly rinsed in ice-cold PBS and snap frozen in liquid nitrogen. Samples were homogenized in 2 ml beat tubes for 20 s at 5,500 g (tissue homogenizer and soft tissue homogenizing CK14–2.0 ml tubes, Precellys, Bertin Instruments, Montigny-le-Bretonneux, France). Each tube contained 200 μl RIPA buffer (Sigma-Aldrich Chemie GmbH, Buchs, Switzerland) per retina and protease inhibitor (1 tablet/10 ml RIPA buffer; cOmplete, EDTA-free Protease Inhibitor Tablets, Roche, Switzerland). After spinning (4°C, 10 min at 2,000 g), 6 μl supernatant was collected and diluted (1:5) in RIPA buffer for the Bradford assay. Next, a glass slide based cytokine antibody microarray was used for quantitative assessment

of cytokine expression (ab197465, Abcam, Cambridge, UK). Each slide provided 16 incubation chambers with the same complete cytokine antibody microarray each. Per array, quadruplicates of antibody spots were provided for all target cytokines, chemokines, and growth factors (GM-CSF, IFN-γ, IL-1α, IL-1β, IL-2, IL-3, IL-4, IL-5, IL-6, IL-9, IL-10, IL-12, IL-13, IL-17, KC, MCP-1, MCSF, RANTES, TNF-α, VEGF). For simplicity, these inflammatory mediators are summarized as cytokines in the following text.

In the quantification process, reference standard solution and protein concentration-matched retinal tissue lysates were diluted with sample diluent according to the manufacturer's instructions. Per experimental group, the solution was incubated in triplicate chambers at room temperature for 2 hr. After washing and drying steps, a glass slide scanner with a Cy3 filter was used for fluorescence intensity detection (ScanRI Microarray Scanner, PerklinElmer, Inc., MA). According to manufacturer's instructions, for each triplicate, the median of the measured intensities was calculated. Further, the mean of the triplicates was used for the subsequent calculations of the final cytokine concentration (pg/ml).

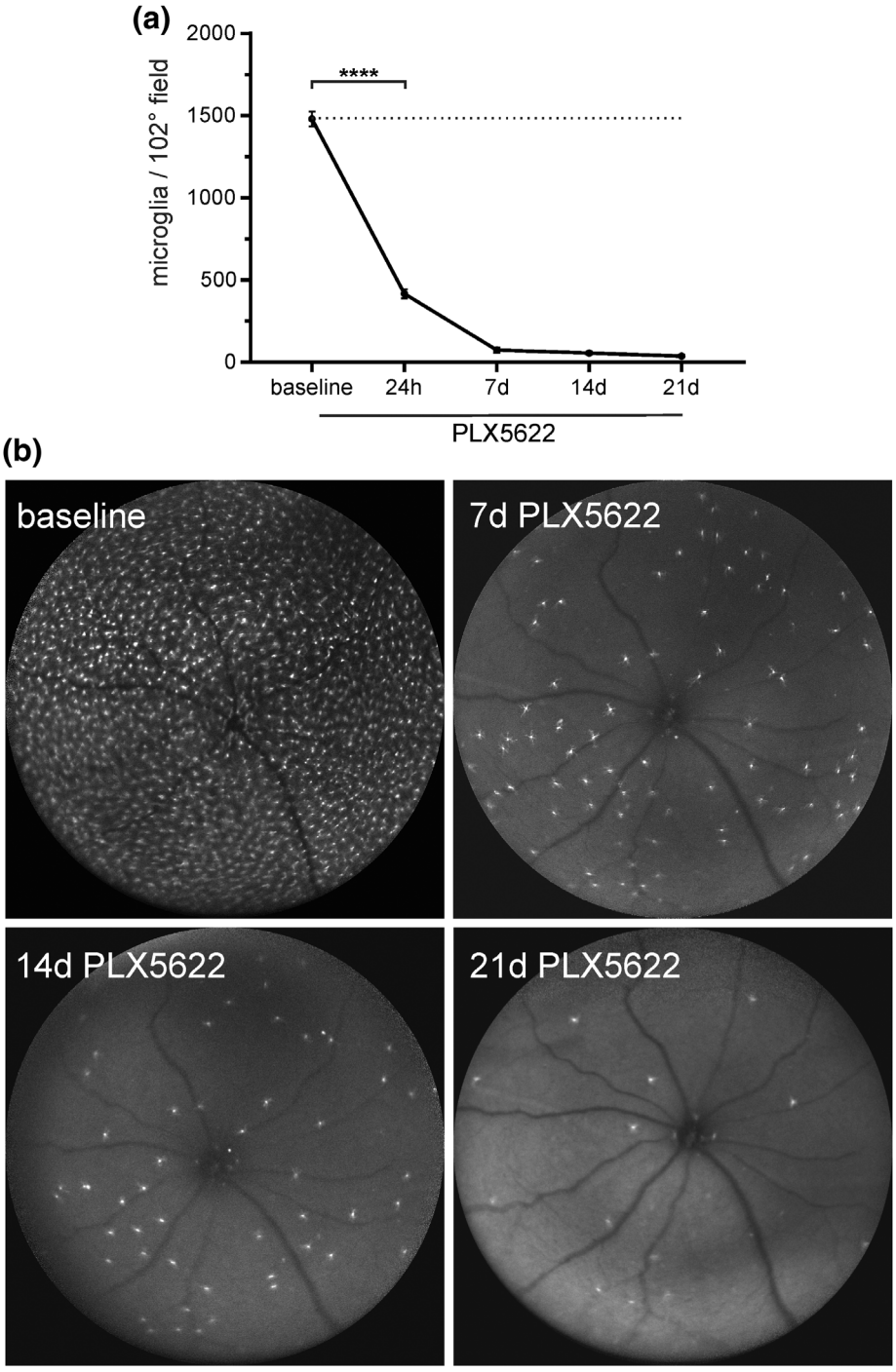

FIGURE 1 Monitoring of retinal microglia depletion by in vivo confocal scanning laser ophthalmoscopy. (a) There is quick and sustained suppression of microglia with PLX5622 treatment. (b) Representative images of microglia depletion kinetics. Pictures were taken in blue-light autofluorescence mode using a 102° ultra-widefield optic at baseline, 7d, 14d, and 21d, ****$p < .0001$ (Dunnett's multiple comparison test)

2.14 | Statistical analysis

The GraphPad Prism 7.03 software (GraphPad Software, Inc., La Jolla, CA) was used for statistical analysis. To analyze microglia depletion, a one-way ANOVA with Tukey's post-hoc test was used. Additionally, 95%-confidential intervals at each time point were calculated.

A two-way ANOVA with Tukey's post-hoc test was used for retinal thickness, RGC survival index and cytokine expression analysis with "time" and "treatment" as factors. To evaluate the effect of PLX5622 on Brn3a$^+$ RGCs, a one-way ANOVA with Holm-Sidak's multiple comparisons test was used. A two-way ANOVA with Sidak's multiple comparison test was performed to analyze semiquantitative

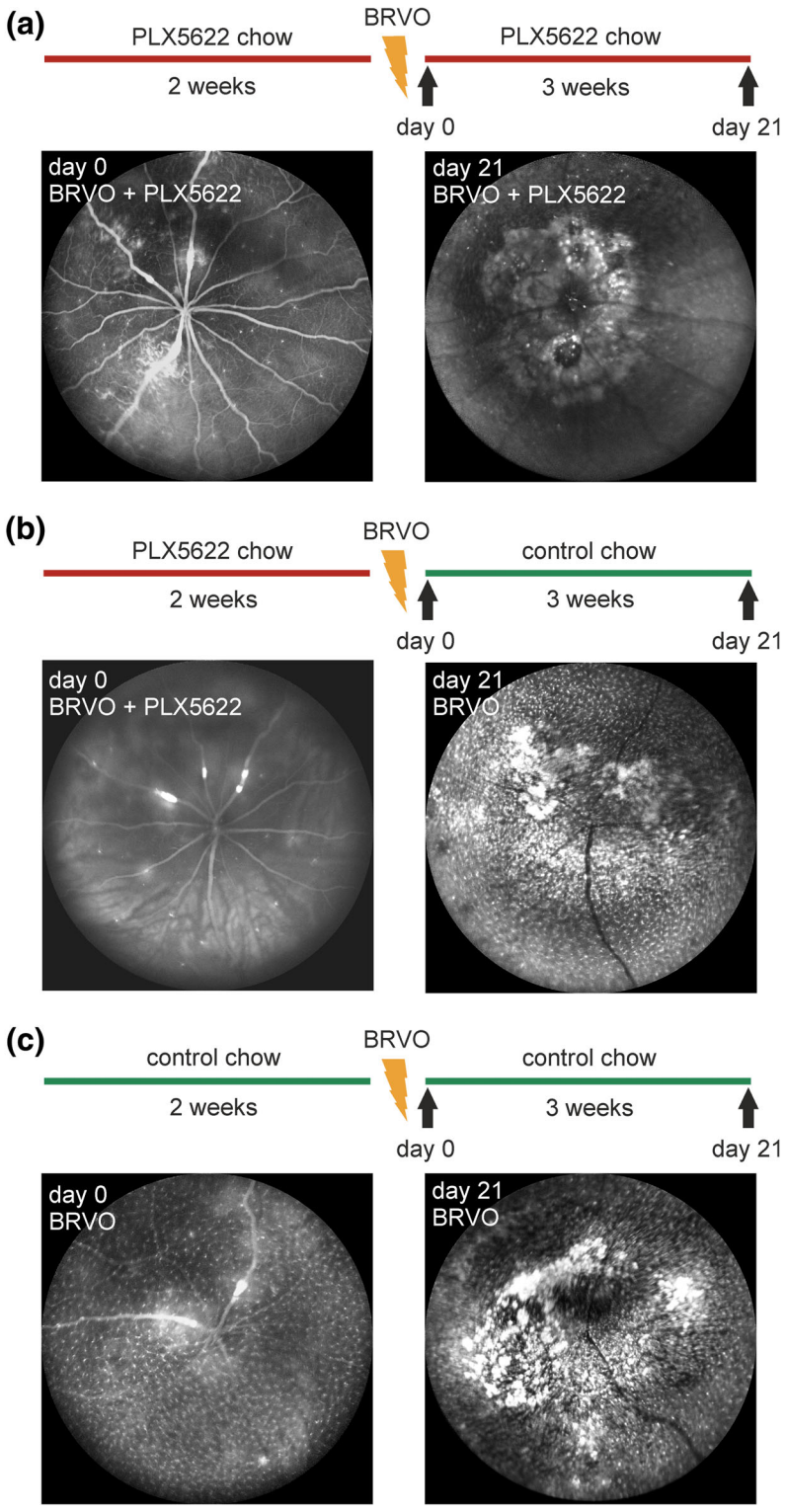

FIGURE 2 Schematic representation of treatment regimen in the three experimental groups and representative in vivo fundus images at baseline and 3 weeks after induction of eBRVO. (a) Animals in the first group were continuously fed with PLX5622 diet (BRVO + PLX5622). Infiltration of GFP$^+$ cells around the optic nerve and targeted blood vessels. (b) In the second group, chow was switched to control diet after induction of retinal vein occlusion (BRVO + Microglia Recovery). In addition to changes visible in the first group, dense repopulation of the retina is noted after 3 weeks. (c) In the third group, eBRVO was induced and mice were continuously kept on control diet (BRVO). Pathologic changes and density of GFP$^+$ cells are similar to those in the second group [Color figure can be viewed at wileyonlinelibrary.com]

grading of Iba1$^+$ cells in the occluded versus nonoccluded parts of the retina, respectively. The significance level was set at $p = .05$. Results are presented as mean ± *SEM*.

3 | RESULTS

3.1 | Kinetics of retinal microglia depletion

Kinetics of microglia depletion were assessed in heterozygous Balb/c *Cx3cr1*$^{gfp/+}$ mice ($n = 9$) by in vivo fundus autofluorescence imaging. All animals were imaged at baseline for microglia counts before the intervention. Using the 102° widefield lens, a mean of 1,481 ± 45.64 cells (95% CI: 1,375–1,586) were counted at baseline per field. Twenty-four hours after initiation of PLX5622 treatment, the result showed a highly significant ($p < .0001$; $n = 9$) reduction to 417.0 ± 27.91 cells (95% CI: 352.6–481.4). One week after continuous PLX5622 treatment, the cell count had further dropped to 74.11 ± 16.75 (95% CI: 35.48–112.7) cells, followed by 55.78 ± 9.46 (95% CI: 33.96–77.59) at 2 weeks and 37.89 ± 5.46 (95% CI: 25.31–50.47) at 3 weeks, respectively. Hence, PLX5622 depleted 95.0% of retinal microglia cells after 1 week of treatment, 96.23% at week two and 97.44% at week three, respectively (Figure 1a,b).

3.2 | Inflammatory cells after experimental BRVO

Three weeks after experimental induction of eBRVO, accumulation of GFP$^+$ cells in continuously depleted mice (BRVO + PLX5622) was primarily seen at the laser sites, where inflammatory cells formed vascular scars (Figure 2a), but GFP$^+$ microglia were virtually absent in the rest of the retina in both occluded and nonoccluded parts. The origin of accumulating cells is difficult to determine. However, since with continuous suppression of microglia in the BRVO + PLX5622 group local proliferation of microglia is unlikely, these cells arguably represent monocytes/macrophages invading from systemic circulation. The two other groups (BRVO + Microglia Recovery, BRVO), in contrast, exhibited abundant presence of GFP$^+$ cells both at the laser site and in surrounding occluded retina (Figure 2b,c). We have previously shown experiments with eBRVO suggesting that in these latter circumstances cells both invade from the systemic circulation but also originate from proliferating residual microglia cells around the site of injury (Ebneter, Kokona, Schneider, et al., 2017). In the nonoccluded parts of the retina, microglia cell density was similar to baseline; however, the microglia exhibited a more amoeboid and activated morphology.

3.3 | PLX5622 delays retinal thinning in ischemic retina

Two-way ANOVA analysis of averaged retinal thickness in occluded and nonoccluded areas had a significant effect on retinal thinning for both factors "treatment" and "time" ($p_{treatment} = .0007$, $p_{time} < .0001$; Figure 3a). Baseline thickness was measured immediately after laser treatment. The average thickness was 247.27 ± 3.50 μm in occluded parts and 242.47 ± 2.62 μm in nonoccluded retina. This was comparable to age-matched treatment naïve Balb/c *Cx3cr1*$^{gfp/+}$ mice ($n = 4$) which had an average retinal thickness of 231.89 ± 12.05 μm. For occluded retina, mice with exposure to PLX5622 (BRVO + PLX5622, BRVO + Microglia Recovery) showed significantly less retinal thickness reduction (around 10%) than untreated mice (25%) 7 days after eBRVO induction (Table 1). During the second week, retinal thinning

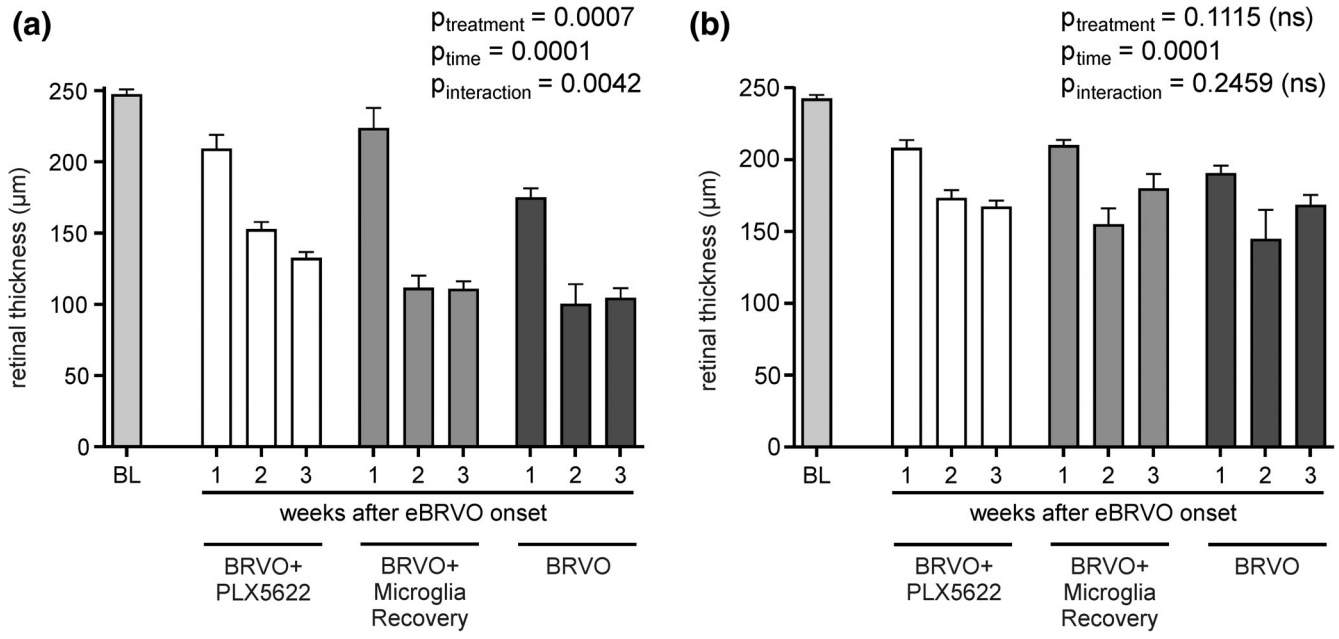

FIGURE 3 Retinal thickness changes in (a) occluded and (b) nonoccluded retinal areas after experimental retinal vein occlusion. Thinning is partially prevented in animals with continuous depletion. Two-way ANOVA confirms that PLX5622 treatment has a significant effect in ischemic retina ($p = .0007$)

TABLE 1 Mean retinal thickness (μm) was measured in the occluded and nonoccluded areas of retinas

Mean retinal thickness														
Occluded area							Nonoccluded area							
	BRVO + PLX5622	BRVO + microglia recovery	BRVO	BRVO + PLX56622 versus BRVO + microglia recovery	*p*-Value	BRVO + PLX562 versus BRVO	*p*-Value	BRVO + microglia recovery versus BRVO	BRVO + PLX5622	BRVO + microglia recovery	BRVO	BRVO + PLX5622 versus BRVO + microglia recovery	*p*-Value	BRVO + PLX5622 versus BRVO	BRVO + microglia recovery versus BRVO
Mean retinal thickness ± *SEM* (μm)					*p*-Value		*p*-Value		Mean retinal thickness ± *SEM* (μm)				*p*-Value		
1w	209.08 ± 9.88	223.58 ± 14.12	174.72 ± 6.57	.4637	.0736		.0112*		208.00 ± 5.73	209.83 ± 3.98	190.49 ± 5.54	.9789	.3053		.2853
	10%	4%	25%						10%	10%	18%				
2w	152.58 ± 5.22	111.37 ± 8.81	100.28 ± 13.89	.0211*	.0121*		.7860		173.25 ± 5.61	154.92 ± 11.19	144.70 ± 20.35	.2591	.0984		.7025
	34%	52%	57%						25%	33%	38%				
3w	132.37 ± 4.44	110.74 ± 5.59	104.49 ± 6.88	.2902	.2223		.9307		167.25 ± 4.39	179.8 ± 10.25	168.34 ± 7.10	.4851	.9960		.6595
	43%	52%	55%						28%	22%	27%				

Note: Measurements were taken for each experimental group (BRVO + PLX5622, BRVO + Microglia Recovery, BRVO) in both areas of the same retina (occluded and nonoccluded) at each time point ($n_{baseline}$ = 46, $n_{treatment}$ = 3–10 eyes/group and time point). Percental change compared to naïve control mice (n = 4) is indicated below each measurement. Two-way ANOVA with factors "treatment" (groups) and "time" was calculated for each area (see Figure 3 for results). This table also shows *p*-values for post-hoc analysis using Tukey's multiple comparison test between groups at each time point for each area. Results are given as mean ± *SEM*, *p < .05.

in BRVO + Microglia Recovery mice rapidly increased and became comparable to untreated mice (around 55%). Thinning in the BRVO + PLX5622 group (34%) was significantly less (p = .0211 and p = .0121, respectively) at this time point. However, 3 weeks after eBRVO induction retinal thinning was no longer statistically different between groups. Interestingly, in nonoccluded areas retinal thinning was also observed (p_{time} < .0001, two-way ANOVA; Figure 3b). However, at no time point was there a significant difference between the different treatment groups (Table 1).

3.4 | PLX5622 protects retinal ganglion cells against cell death in ischemic retina

For whole mounted retinas, the relative retinal ganglion cell density visualized by Brn3a immune-staining (RGC survival index) was calculated at all-time points. Two-way ANOVA for both factors, PLX5622 "treatment" and "time", showed a significant effect on RGC density ($p_{treatment}$ = .0004, p_{time} = .0001; Figure 4).

Two weeks after eBRVO, continuously PLX5622 treated animals had significantly higher RGC survival (p = .0053; Table 2) compared to nondepleted animals (BRVO), translating to a 71.4% higher survival rate of RGCs in the PLX5622 treated group (Table 2 and Figure 4). A similar result was noted 3 weeks after eBRVO (49.2% higher survival, p = .0434; Figure 5).

To assess whether PLX5622 directly affects Brn3a labeling, baseline Brn3a RGC counts were determined in six whole mounted retinas revealing a mean cell count of 43,912 ± 880 RGCs per retina (CI 95%: 41,649–46,175). This result was compared to three PLX5622 treated retinas per group and time point at 1, 2, and 3 weeks of treatment (data not shown). One-way ANOVA showed no significant reduction in total RGC counts at all three time points ($p_{treatment}$ = .7697),

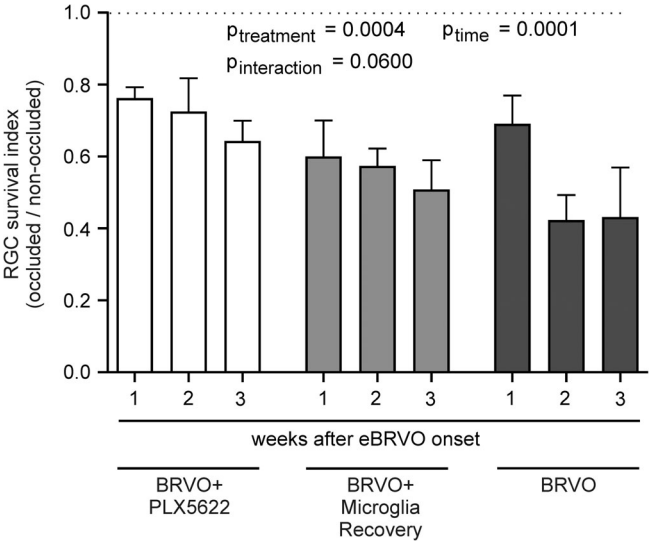

FIGURE 4 Retinal ganglion cells are partially salvaged in PLX5622 treated mice. Two-way ANOVA confirms that treatment affords significant protection in the ischemic retina

suggesting that PLX5622 itself did not affect Brn3a labeling of RGCs during the period of observation.

3.5 | Spatiotemporal microglia distribution in occluded and nonoccluded retina

Semiquantitative retinal section analysis showed for occluded and nonoccluded areas the highest microglia density in PLX5622 naïve animals (BRVO), while microglia were absent at all time points in the BRVO+PLX5622 group and intermediate in the BRVO + Microglia Recovery group (Figure 6a,b). Hence, in both areas, two-way ANOVA with factors PLX5622 "treatment" and "time" showed overall a significant effect for PLX5622 treatment (occluded area: $p_{treatment} < .0001$; nonoccluded area: $p_{treatment} < .0001$). Further, in the occluded area, Tukey's multiple comparison showed significant microglia/macrophage density differences between the BRVO and the BRVO + Microglia Recovery group at the first and second week after eBRVO ($p_{1week} = .0015$, $p_{2weeks} = .0037$). In the latter group, at the latest time point of observation, microglia recovery reached almost the microglia density of the BRVO group and did not show any significant difference anymore (Figure 6a). In nonoccluded areas, microglia recovered faster and the difference to the BRVO group was only significant at time point 1 week ($p_{1week} = .0011$; Figure 6b).

The difference of microglia density between areas (occluded vs. nonoccluded) within the same treatment groups was not significant (Figure 6c,d). Although in the BRVO + Microglia Recovery group the two-way ANOVA test showed global significance ($p_{area} = .0090$, $p_{time} = .0011$), in post-hoc multiple comparisons the individual differences were not statistically significant (Figure 6c). Intriguingly, microglia density seemed at all-time points higher in nonoccluded

TABLE 2 The retinal ganglion cell (RGC) survival index was defined as the relative density of Brn3a$^+$ RGCs in the occluded area relative to the nonoccluded area of retinal flat mounts after experimental branch vein occlusion

RGC survival index						
	BRVO + PLX5622	BRVO + microglia recovery	BRVO	BRVO + PLX5622 versus BRVO + microglia recovery	BRVO + PLX5622 versus BRVO	BRVO + microglia recovery versus BRVO
	RGC survival index			*p*-Value	*p*-Value	*p*-Value
1w	0.762 ± 0.031	0.600 ± 0.101	0.690 ± 0.079	.0294*	.6425	.5511
2w	0.725 ± 0.093	0.574 ± 0.048	0.423 ± 0.070	.1147	.0053**	.1714
3w	0.643 ± 0.056	0.508 ± 0.081	0.431 ± 0.138	.1695	.0434*	.6647

Note: Two-way ANOVA with factors "treatment" (groups) and "time" was used (see Figure 4 for results). This table shows actual RGC survival indices and *p*-values for post-hoc analysis using Tukey's multiple comparison between groups at each time point. Results are given as mean ± *SEM*, *$p < .05$, **$p < .01$.

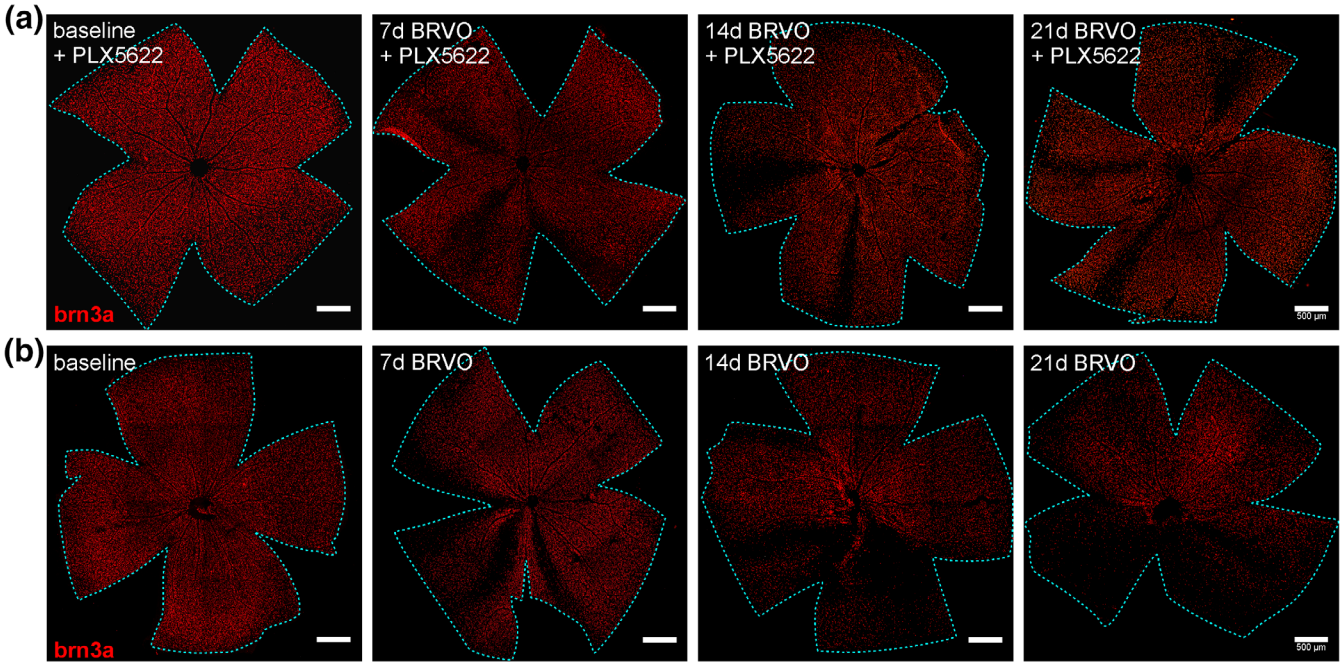

FIGURE 5 Representative examples of retinal whole mounted retinas stained for retinal ganglion cells (Brn3a) in (a) continuously depleted mice (BRVO + PLX5622) and (b) control mice (BRVO) at baseline, 7d, 14d, and 21d after eBRVO induction. Scale bars, 500 µm [Color figure can be viewed at wileyonlinelibrary.com]

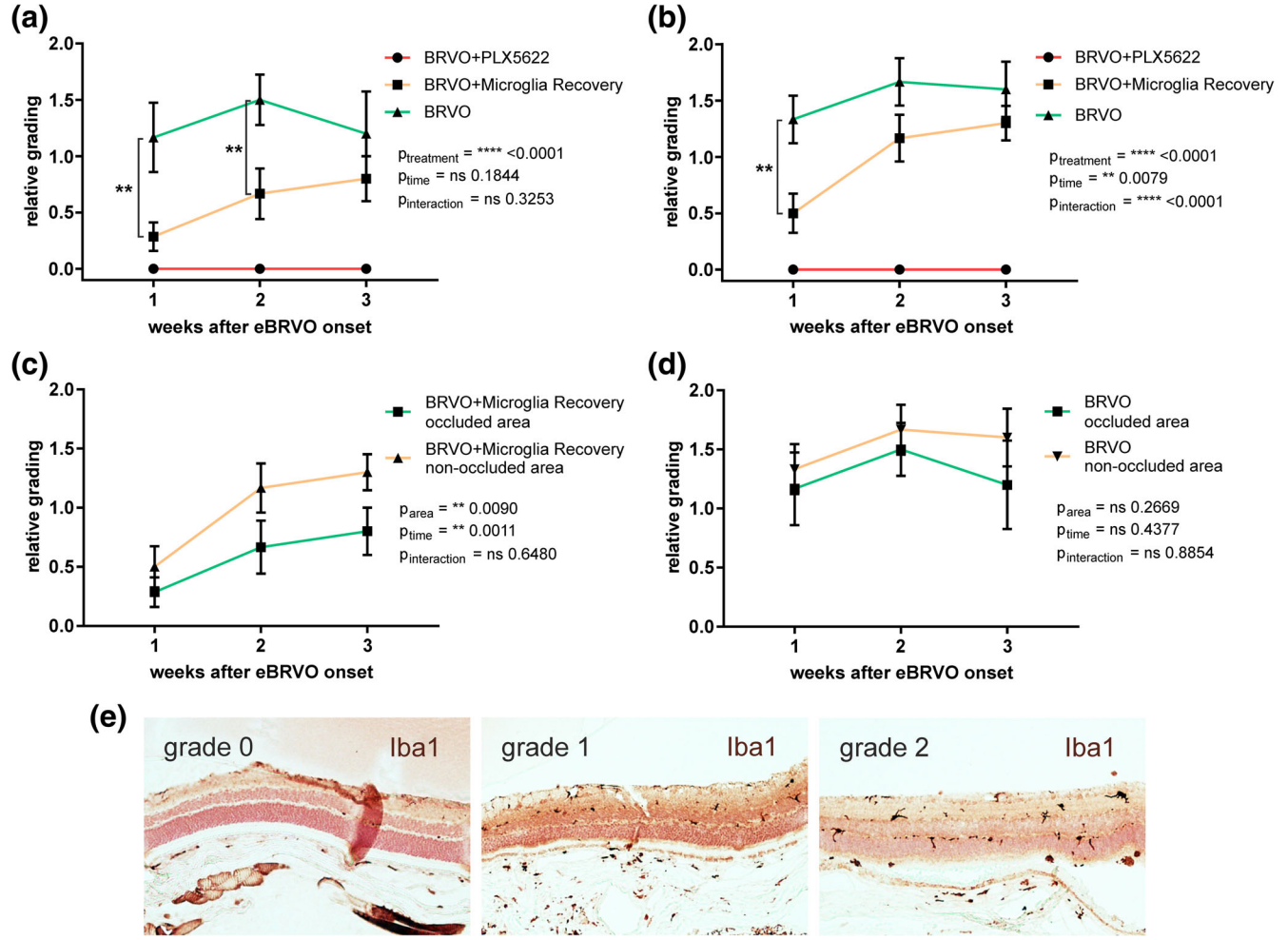

FIGURE 6 Semiquantitative grading of microglia repopulation in (a) occluded and (b) nonoccluded retina. (c) Analysis for all animals with cessation of treatment at time of laser (BRVO + Microglia Recovery) and (d) control mice. Templates used for grading are shown in (e). *P*-Values are shown for two-way ANOVA with factors "treatment" and "time." *p < .05, **p < .01, p < .001, ****p < .0001 [Color figure can be viewed at wileyonlinelibrary.com]

areas in both the BRVO + Microglia Recovery and the BRVO group, although not statistically significant (Figure 6c,d).

3.6 | Microglia/macrophage depletion reduces inflammatory cytokines in ischemic retina

To evaluate changes of retinal cytokine expression, a quantitative cytokine microarray including 20 cytokines was performed 24 and 72 hr after eBRVO. PLX5622 treatment led to significant changes for all cytokines evaluated (Table S1).

The graphic representations with multiple comparisons of the most relevant proinflammatory (IFN-γ, TNF-α, IL-1β, IL-6, VEGF, IL-12, MCP-1) and anti-inflammatory cytokines (IL-4, IL-10, IL-13) are shown in Figure 7a,b, respectively.

All selected proinflammatory cytokines (Figure 7a) with exception of IL-12 were significantly decreased in the BRVO + PLX5622 group compared to the BRVO group ($p_{IFN\text{-}\gamma}$ = .0205; $p_{TNF\text{-}\alpha}$ = .0055; $p_{IL\text{-}1\beta}$ < .0278; $p_{IL\text{-}6}$ < .0001; p_{VEGF} < .0001; $p_{IL\text{-}12}$ = .3777; $p_{MCP\text{-}1}$ < .0001) 24 hr after eBRVO induction. Except for IL-6, VEGF, and IL-12, cytokine levels were in fact similar to baseline expression measured in naïve control mice. Suppression of cytokine levels in BRVO + PLX5622 mice was even more pronounced 72 hr with levels significantly below baseline, except VEGF ($p_{IFN\text{-}\gamma}$ < .0001; $p_{TNF\text{-}\alpha}$ < .0001; $p_{IL\text{-}1\beta}$ = .0002; $p_{IL\text{-}6}$ = .0013; $p_{IL\text{-}12}$ < .0001; $p_{MCP\text{-}1}$ < .0001).

For both time points, proinflammatory cytokine levels were comparable between the BRVO + Microglia Recovery group and the BRVO group. The only exceptions were IL-6, IL-12, VEGF, and MCP-1 at the 24 hr time point, when for IL-6, VEGF, and MCP-1 levels were close to expression in the microglia-depleted group (BRVO + PLX5622) and, thus, significantly decreased compared to the BRVO group ($p_{IL\text{-}6}$ < .0001; p_{VEGF} = .0001; $p_{MCP\text{-}1}$ < .0001). At the 24 hr time point, IL-12 was highly upregulated in the BRVO + Microglia Recovery group compared to the BRVO + PLX5622 ($p_{IL\text{-}12}$ = .0022) and the BRVO group ($p_{IL\text{-}12}$ = .0261), respectively.

IL-4, IL-10, and IL-13 are involved in microglia/macrophage-dependent anti-inflammatory signaling, and IL-10 in addition has an autocrine effect that strongly downregulates the proinflammatory cytokine burst (Anderson & Mosser, 2002; Gordon, 2003). Two-way

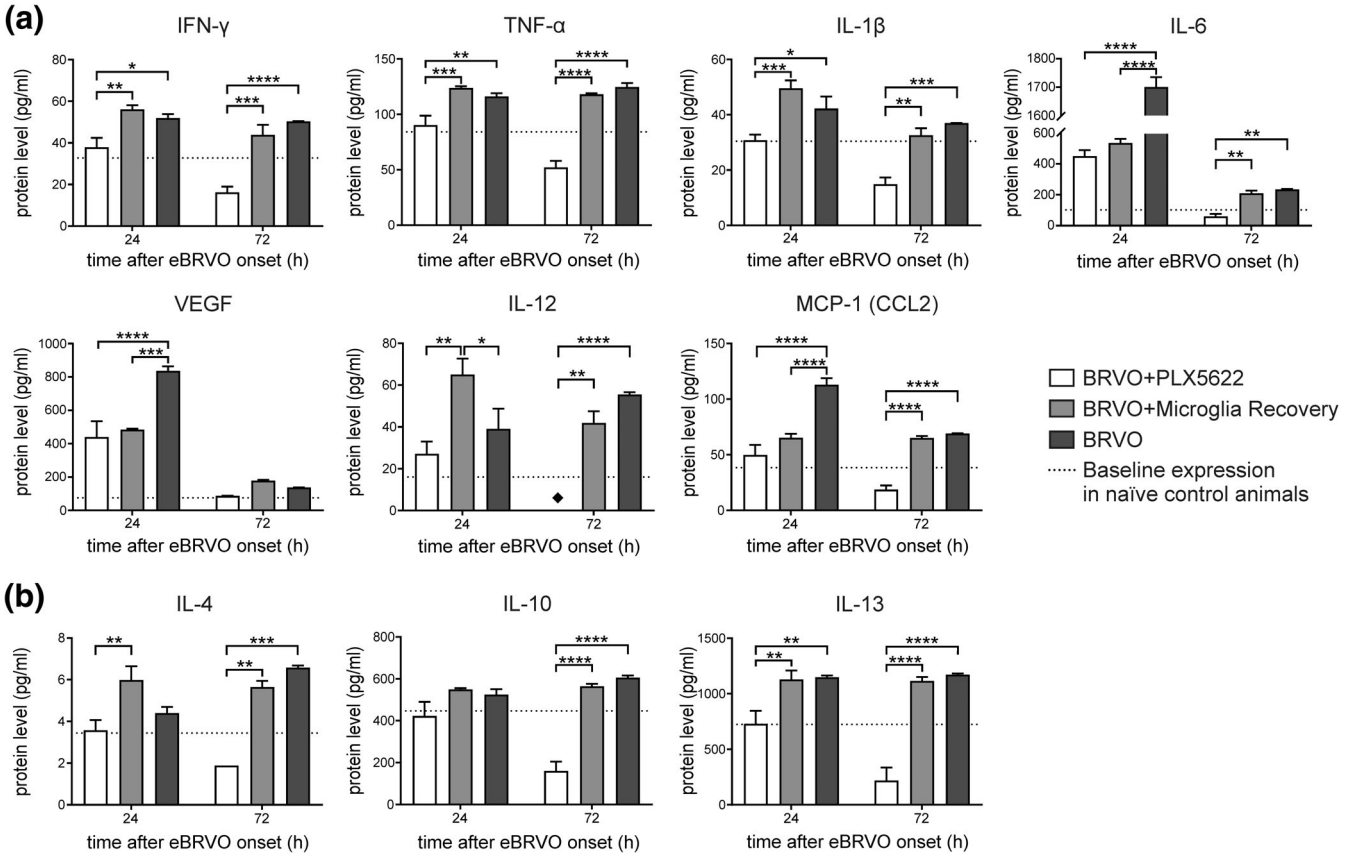

FIGURE 7 Results from mouse cytokine antibody microarray for a selection of (a) proinflammatory and (b) anti-inflammatory proteins. Significance levels: *$p < .05$, **$p < .01$, ***$p < .001$, ****$p < .0001$; ◆: expression level below detection threshold (0.1 pg/ml)

ANOVA showed for all three cytokines significant differences for the factor "treatment" ($p_{IL\text{-}4} = .0003$; $p_{IL\text{-}10} < .0001$; $p_{IL\text{-}13} < .0001$). Protein levels of the anti-inflammatory cytokines IL-4, IL-10, and IL-13 were close to baseline in the continuously depleted BRVO + PLX5622 group 24 hr after eBRVO, and even fell lower at 72 hr (Figure 7b). Multiple comparison revealed that protein levels of IL-4 and IL-10 in the BRVO + PLX5622 group were not even significantly different from the BRVO group 24 hr after eBRVO induction, whereas IL-13 was significantly lower ($p_{IL\text{-}4} = .3827$; $p_{IL\text{-}10} = .1243$; $p_{IL\text{-}13} = .0033$). However, all three proteins were significantly decreased at the 72 hr time point ($p_{IL\text{-}4} = .0006$; $p_{IL\text{-}10} < .0001$; $p_{IL\text{-}13} < .0001$). The protein levels of IL-10 and IL-13 in the BRVO + Microglia Recovery group were at both time points similar to the BRVO group. Of note, 24 hr after eBRVO onset, the protein level of IL-4 in the BRVO + Microglia Recovery group was increased compared to the BRVO group, although not significantly ($p_{IL\text{-}4} = .0533$).

4 | DISCUSSION

Microglia have been shown to have ambiguous effects on retinal pathologies and are capable of producing both pro- and anti-inflammatory mediators upon activation. In this study, we investigated whether PLX5622-induced microglia depletion has an impact on retinal damage after eBRVO.

We were able to show that CSF1R-mediated depletion of microglia resulted in a diminished proinflammatory innate immune response and in a delay of retinal thinning that was associated with greater RGC survival. Of note, PLX5622 cessation at the time of experimental vein occlusion resulted in only minimal RGC protection.

It has been shown in retinas with eBRVO, that the presence of activated microglia and bone marrow-derived invading macrophages is significantly increased early, lasting for at least 4 weeks (Ebneter, Kokona, Schneider, et al., 2017). This increased presence of activated microglia and/or macrophages is consistent with the higher number of GFP^+ cells observed in our in vivo SLO images of non-PLX5622 treated or recovering animals (Figure 2b,c). In line, we have also shown that several potent proinflammatory cytokines such as IFN-γ, TNF-α, IL-1β, IL-6, IL-12, and MCP-1 are greatly increased in non-PLX5622 treated ischemic retinas. On the other hand, microglia-depleted retinas did not only show a decrease in GFP^+ cells but also in proinflammatory cytokine expression. In our previous study, we also have shown that INF-γ and TNF-α peak early after eBRVO (Ebneter, Kokona, Schneider, et al., 2017). INF-γ directly increases TNF-α production in microglia or macrophages (Welser-Alves & Milner, 2013), while TNF-α itself has an autocrine activation mechanism on microglia via a positive feedback loop (Kuno et al., 2005). In the CNS, activated

microglia cells and macrophages are one of the major sources of TNF-α and other proinflammatory mediators like IL-1β, IL-6, reactive oxygen species, and nitric oxide (NO; Mantovani et al., 2004; Natoli et al., 2017; A. R. Patel, Ritzel, McCullough, & Liu, 2013; Rivera et al., 2013; Welser-Alves & Milner, 2013). Nakazawa et al. demonstrated in a glaucoma model that ocular hypertension increase TNF-α levels in the retina following microglia activation. Subsequently, oligodendrocytes in the optic nerve die and leave vulnerable demyelinated RGC axons behind. Proinflammatory mediators damage these free axons causing death to the corresponding RGCs. Interestingly, microglia deficient mice showed no RGC loss after induction of ocular hypertension or after TNF-α injection, suggesting that microglia and TNF-α playing a key role in RGC death (Nakazawa et al., 2006; S. Patel & Player, 2009). Another experimental glaucoma study used Etanercept, an inhibitor of TNF-α and TNF-β, showing that inhibition of microglia activation resulted in mitigation of axonal degeneration and RGC loss (Roh et al., 2012). In accordance with these findings, we postulate that part of the protection of RGCs in microglia-depleted animals results from reduced secretion of proinflammatory cytokines and harmful mediators like TNF-α or IL-1β.

Other studies reported findings similar to outcomes of our experiments with increased RGC survival after microglia suppression. Two studies demonstrated reduced microglia activation using low-dose minocycline in a retinal ischemia–reperfusion injury mouse and rat model of BRVO, respectively; both studies found reduced RGC loss (R. Huang, Liang, et al., 2018; Sun et al., 2013). A third study by Takeda et al. showed increased RGC survival in minocycline and PLX5622 treated mice after NMDA injection causing excitotoxicity in RGCs (Takeda et al., 2018). The proposed neuroprotective mechanism of minocycline, a broad-spectrum tetracycline antibiotic, and PLX5622 is that by inhibition of microglia the secretion of proinflammatory cytokines such as TNF-α, IL-1β, and IL-6 is diminished (Plane, Shen, Pleasure, & Deng, 2010; Stirling, Koochesfahani, Steeves, & Tetzlaff, 2005; Takeda et al., 2018). The first two studies demonstrated not only protection against RGC loss but also some preservation of signals in electroretinograms, indicating preservation of function in minocycline treated retinas. Since PLX5622 ablates microglia almost completely in the CNS and retina (Elmore et al., 2014; Hilla, Diekmann, & Fischer, 2017; Takeda et al., 2018), and our findings corroborate a decrease in several proinflammatory cytokines, it is plausible that the mentioned neurodegenerative processes involve activated microglia that are significantly altered in PLX5622 treated retinas. Reduced influx of inflammatory cells from the circulation might be among the reasons for increased RGC survival in PLX5622 treated animals. It is worth mentioning that it is not yet clear why some microglia "escape" CSF1-R inhibition, but this observation has been made by several groups (Acharya et al., 2016; Hilla et al., 2017; Y. Huang, Xu, et al., 2018; Takeda et al., 2018), and depletion is not complete. Some authors speculate that escaping cells are a subpopulation of microglia that do not express nor depend on CSF1R signaling (Paschalis et al., 2018; Unger, Schernthaner, Marschallinger, Mrowetz, & Aigner, 2018). However, after 2 weeks of PLX5622 treatment (time point of eBRVO), apparent microglia density was only about 3% of baseline. Despite some residual microglia, we consider this meaningful depletion with relevant biological effects.

Evidence from brain pathology after hypoxic insults indicate another potential mechanism. Infiltrating lymphocytes, especially γδT cells play a crucial role in the secondary progression of brain injury after infarction (Iadecola & Anrather, 2011; Shichita et al., 2009). This subpopulation of T cells does not need stimulation by the antigen-specific T-cell receptor to be activated and to secret (as the main source in CNS) the cytotoxic cytokine IL-17. In fact, γδT cells are directly activated by IL-23, which is mostly secreted by infiltrating macrophages and activated microglia (Shichita et al., 2009). Finally, Shichita et al. (2009) showed that deletion of γδT cells successfully reduces infarct size. Our experiments showed efficient downregulation of IL-17 3 days after eBRVO in continuously PLX5622 treated mice (Table S1). However, there is evidence that activated retinal microglia can also have direct protective effects on RGCs. Sappington et al. (2006) have shown in vitro that microglia-derived factors, in particular IL-6, protected RGCs against pressure-induced apoptosis. Further, Chidlow et al. has demonstrated that osteopontin produced by microglia protects RGCs from ischemic and excitotoxic damage (Chidlow, Wood, Manavis, Osborne, & Casson, 2008).

Since BRVO is not primarily an inflammatory disease, vasogenic mediators are also elevated in BRVO affected retinas. In humans suffering from BRVO and macular edema, increased levels of vascular factors were measured in the vitreous, such as VEGF, soluble intracellular adhesion molecule (sICAM), IL-6, or monocyte chemotactic protein 1 (MCP-1) (Noma, Mimura, & Eguchi, 2013). In these BRVO patients, via hypoxic inducible factor 1α (HIF-1α), retinal hypoxia leads to upregulated secretion of VEGF in vascular endothelial cells, astrocytes, and Müller cells (Kaur, Sivakumar, & Foulds, 2006). Consequently, VEGF increases vascular permeability of the blood–retina barrier (Kaur et al., 2006; Mayhan, 1999), causing vasogenic edema and an efflux of inflammatory factors into the vitreous (Noma et al., 2013). Corroborating these findings in humans with BRVO, we also found highly increased protein levels of VEGF, IL-6, and MCP-1 after eBRVO (Figure 7a). To our knowledge, PLX5622 should not directly affect secretion from other cells such as vascular endothelium or Müller cells. These cells are known to produce VEGF and/or IL-6. This might be the reason for lack of early downregulation to baseline expression in PLX5622 treated animals compared to microglia specific cytokines such as TNF-α or IL-1β that are swiftly suppressed. Thus, deleterious effects of blood–retina barrier breakdown are not completely abolished by microglia depletion.

Importantly, in a model of pure retrograde axonal degeneration microglia/monocyte inhibition did not change RGC survival. Hilla et al. (2017) showed that PLX5622-induced microglia depletion had neither a protective nor an exacerbating effect on RGC survival after optic nerve crush. However, reactive changes of astrocytes that are closely related to RGC axons were not examined. Chan-Ling et al. (1991) have shown that optic nerve crush in kitten caused reactive distribution and morphology changes of astrocytes. Hilla et al. stated that the removal of RGC remnants was impaired upon PLX5622 treatment and postulated the necessity of activated microglia for this process. In the

eBRVO model ischemia causes breakdown of the blood-retinal barrier which is composed of endothelium, basal lamina and astrocyte endfeet. Inhibition of microglia may not directly influence astrocyte dysfunction, which arguably contributes significantly to blood-retinal barrier breakdown, but indirect interactions are complex.

A major limitation of this study is that we cannot clearly distinguish between activated microglia and infiltrating monocytes (macrophages). An approach using anti-tmem119 and anti-CD163 staining (Zhou et al., 2017) seems not helpful in our setting since recent papers have shown that tmem119 is quickly downregulated in activated CNS microglia (Keren-Shaul et al., 2017; Krasemann et al., 2017; Ronning, Karlen, Miller, & Burns, 2019). In fact, our own tests with these antibodies (not shown) were not fruitful in addressing this issue. Furthermore, staining infiltrating macrophages with CD163 might even be misleading because CD163, presumably a hemoglobin scavenger receptor, is not only expressed on blood/derived macrophages/monocytes but also on resident microglia (Lim, Hainsworth, Mohan, & Chaurasia, 2019; Pey, Pearce, Kalaitzakis, Griffin, & Gentleman, 2014; Poon et al., 2019; Vogel et al., 2013). Flow cytometry might provide further insight here but was not in the scope of the current project. Nevertheless, PLX5622 depletes microglia and, at least to our knowledge, also affects infiltrated macrophages (Feng et al., 2017). Moreover, in this study, we depleted microglia/macrophages for a short period of time. It is still controversial, whether long-term microglia/macrophages depletion might be detrimental for synaptic integrity. Another limitation might be a disturbed rheology in the whole retina after laser application to specific retinal veins. Such changes might explain retinal thinning of areas not directly in the drainage area of occluded veins (Figure 3b). Nevertheless, in order to analyze imaging data in a meaningful way, we had to assume that conditions were presumably stable in parts of the retina not directly involved in eBRVO, which allowed to define the "RGC survival index." By using this ratio, we normalize RGC loss data using an internal reference/control, thus eliminating general RGC damage caused by widespread rheology changes, degeneration of the retina associated with aging, light toxicity, or other unknown factors inherent to the model homogeneously affecting the entire retina.

In summary, we found that short-term microglia depletion delays atrophy of the inner retinal layers and reduces retinal ganglion cell loss in the experimentally occluded retina. The protective mechanism might be mediated by downregulation of the innate immune response resulting in fewer activated microglia/macrophages and, thus, hampered early proinflammatory cytokine release, ultimately mitigating blood–retina barrier breakdown. Nevertheless, the protective effect was limited. Further study is needed to elucidate the complex interplay between neurons, glia and inflammatory cells in the hypoxic neuroretina.

ACKNOWLEDGMENTS

We thank Stephanie Lötscher-Jovanovic and Anelia Schweri-Olac for technical assistance. We specially thank Aliu Nijas from the Department of Human Genetics, Inselspital, Bern University Hospital, Switzerland, for providing the glass slide scanner and technical assistance. PLX5622 rodent diet was provided without financial support under a Materials Transfer Agreement with Plexxikon Inc., Berkeley, CA. This project was funded by CTU Research-Grant (84800858; AE), the Prix Retina 2016 grant (AE), and by an unrestricted grant from Dr. Streuli-Fonds (AE), all in Bern, Switzerland. Xuan Liu is awardee of a Swiss Government Excellence Scholarship (2017.0620) and supported by the Chinese Scholarship Council (201600160105).

DATA AVAILABILITY STATEMENT

The data that support the findings of this study are available from the corresponding author upon reasonable request.

ORCID

Joël Jovanovic https://orcid.org/0000-0002-9195-2239
Despina Kokona https://orcid.org/0000-0002-6235-1266
Martin S. Zinkernagel https://orcid.org/0000-0002-5622-114X
Andreas Ebneter https://orcid.org/0000-0001-6666-2558

REFERENCES

Acharya, M. M., Green, K. N., Allen, B. D., Najafi, A. R., Syage, A., Minasyan, H., … Limoli, C. L. (2016). Elimination of microglia improves cognitive function following cranial irradiation. *Scientific Reports*, *6*, 31545. https://doi.org/10.1038/srep31545

Anderson, C. F., & Mosser, D. M. (2002). A novel phenotype for an activated macrophage: The type 2 activated macrophage. *Journal of Leukocyte Biology*, *72*(1), 101–106.

Berti, R., Williams, A. J., Moffett, J. R., Hale, S. L., Velarde, L. C., Elliott, P. J., … Tortella, F. C. (2002). Quantitative real-time RT-PCR analysis of inflammatory gene expression associated with ischemia-reperfusion brain injury. *Journal of Cerebral Blood Flow and Metabolism*, *22*(9), 1068–1079. https://doi.org/10.1097/00004647-200209000-00004

Chan-Ling, T., & Stone, J. (1991). Factors determining the migration of astrocytes into the developing retina: Migration does not depend on intact axons or patent vessels. *The Journal of Comparative Neurology*, *303*(3), 375–386. https://doi.org/10.1002/cne.903030304

Chen, Y., Hallenbeck, J. M., Ruetzler, C., Bol, D., Thomas, K., Berman, N. E., & Vogel, S. N. (2003). Overexpression of monocyte chemoattractant protein 1 in the brain exacerbates ischemic brain injury and is associated with recruitment of inflammatory cells. *Journal of Cerebral Blood Flow and Metabolism*, *23*(6), 748–755. https://doi.org/10.1097/01.WCB.0000071885.63724.20

Chidlow, G., Wood, J. P., Manavis, J., Osborne, N. N., & Casson, R. J. (2008). Expression of osteopontin in the rat retina: Effects of excitotoxic and ischemic injuries. *Investigative Ophthalmology & Visual Science*, *49*(2), 762–771. https://doi.org/10.1167/iovs.07-0726

Clausen, B. H., Lambertsen, K. L., Babcock, A. A., Holm, T. H., Dagnaes-Hansen, F., & Finsen, B. (2008). Interleukin-1beta and tumor necrosis factor-alpha are expressed by different subsets of microglia and macrophages after ischemic stroke in mice. *Journal of Neuroinflammation*, *5*, 46. https://doi.org/10.1186/1742-2094-5-46

Dagher, N. N., Najafi, A. R., Kayala, K. M., Elmore, M. R., White, T. E., Medeiros, R., … Green, K. N. (2015). Colony-stimulating factor 1 receptor inhibition prevents microglial plaque association and improves

cognition in 3xTg-AD mice. *Journal of Neuroinflammation*, *12*, 139. https://doi.org/10.1186/s12974-015-0366-9

Dharmarajan, S., Fisk, D. L., Sorenson, C. M., Sheibani, N., & Belecky-Adams, T. L. (2017). Microglia activation is essential for BMP7-mediated retinal reactive gliosis. *Journal of Neuroinflammation*, *14*(1), 76. https://doi.org/10.1186/s12974-017-0855-0

Ebneter, A., Agca, C., Dysli, C., & Zinkernagel, M. S. (2015). Investigation of retinal morphology alterations using spectral domain optical coherence tomography in a mouse model of retinal branch and central retinal vein occlusion. *PLoS One*, *10*(3), e0119046. https://doi.org/10.1371/journal.pone.0119046

Ebneter, A., Kokona, D., Jovanovic, J., & Zinkernagel, M. S. (2017). Dramatic effect of oral CSF-1R kinase inhibitor on retinal microglia revealed by in vivo scanning laser ophthalmoscopy. *Translational Vision Science & Technology*, *6*(2), 10. https://doi.org/10.1167/tvst.6.2.10

Ebneter, A., Kokona, D., Schneider, N., & Zinkernagel, M. S. (2017). Microglia activation and recruitment of circulating macrophages during ischemic experimental branch retinal vein occlusion. *Investigative Ophthalmology & Visual Science*, *58*(2), 944–953. https://doi.org/10.1167/iovs.16-20474

Ehlken, C., Grundel, B., Michels, D., Junker, B., Stahl, A., Schlunck, G., … Pielen, A. (2015). Increased expression of angiogenic and inflammatory proteins in the vitreous of patients with ischemic central retinal vein occlusion. *PLoS One*, *10*(5), e0126859. https://doi.org/10.1371/journal.pone.0126859

Elmore, M. R., Najafi, A. R., Koike, M. A., Dagher, N. N., Spangenberg, E. E., Rice, R. A., … Green, K. N. (2014). Colony-stimulating factor 1 receptor signaling is necessary for microglia viability, unmasking a microglia progenitor cell in the adult brain. *Neuron*, *82*(2), 380–397. https://doi.org/10.1016/j.neuron.2014.02.040

Erblich, B., Zhu, L., Etgen, A. M., Dobrenis, K., & Pollard, J. W. (2011). Absence of colony stimulation factor-1 receptor results in loss of microglia, disrupted brain development and olfactory deficits. *PLoS One*, *6*(10), e26317. https://doi.org/10.1371/journal.pone.0026317

Feng, X., Valdearcos, M., Uchida, Y., Lutrin, D., Maze, M., & Koliwad, S. K. (2017). Microglia mediate postoperative hippocampal inflammation and cognitive decline in mice. *JCI Insight*, *2*(7), e91229. https://doi.org/10.1172/jci.insight.91229

Fleming, J. C., Norenberg, M. D., Ramsay, D. A., Dekaban, G. A., Marcillo, A. E., Saenz, A. D., … Weaver, L. C. (2006). The cellular inflammatory response in human spinal cords after injury. *Brain*, *129*(Pt 12), 3249–3269. https://doi.org/10.1093/brain/awl296

Ginhoux, F., Greter, M., Leboeuf, M., Nandi, S., See, P., Gokhan, S., … Merad, M. (2010). Fate mapping analysis reveals that adult microglia derive from primitive macrophages. *Science*, *330*(6005), 841–845. https://doi.org/10.1126/science.1194637

Gomez-Nicola, D., Fransen, N. L., Suzzi, S., & Perry, V. H. (2013). Regulation of microglial proliferation during chronic neurodegeneration. *The Journal of Neuroscience*, *33*(6), 2481–2493. https://doi.org/10.1523/jneurosci.4440-12.2013

Gordon, S. (2003). Alternative activation of macrophages. *Nature Reviews. Immunology*, *3*(1), 23–35. https://doi.org/10.1038/nri978

Guadagno, J., Xu, X., Karajgikar, M., Brown, A., & Cregan, S. P. (2013). Microglia-derived TNFalpha induces apoptosis in neural precursor cells via transcriptional activation of the Bcl-2 family member puma. *Cell Death & Disease*, *4*, e538. https://doi.org/10.1038/cddis.2013.59

Hilla, A. M., Diekmann, H., & Fischer, D. (2017). Microglia are irrelevant for neuronal degeneration and axon regeneration after acute injury. *The Journal of Neuroscience*, *37*(25), 6113–6124. https://doi.org/10.1523/jneurosci.0584-17.2017

Huang, R., Liang, S., Fang, L., Wu, M., Cheng, H., Mi, X., & Ding, Y. (2018). Low-dose minocycline mediated neuroprotection on retinal ischemia-reperfusion injury of mice. *Molecular Vision*, *24*, 367–378.

Huang, Y., Xu, Z., Xiong, S., Sun, F., Qin, G., Hu, G., … Peng, B. (2018). Repopulated microglia are solely derived from the proliferation of residual microglia after acute depletion. *Nature Neuroscience*, *21*(4), 530–540. https://doi.org/10.1038/s41593-018-0090-8

Hume, D. A., & MacDonald, K. P. (2012). Therapeutic applications of macrophage colony-stimulating factor-1 (CSF-1) and antagonists of CSF-1 receptor (CSF-1R) signaling. *Blood*, *119*(8), 1810–1820. https://doi.org/10.1182/blood-2011-09-379214

Iadecola, C., & Anrather, J. (2011). The immunology of stroke: From mechanisms to translation. *Nature Medicine*, *17*(7), 796–808. https://doi.org/10.1038/nm.2399

Jung, S., Aliberti, J., Graemmel, P., Sunshine, M. J., Kreutzberg, G. W., Sher, A., & Littman, D. R. (2000). Analysis of fractalkine receptor CX(3) CR1 function by targeted deletion and green fluorescent protein reporter gene insertion. *Molecular and Cellular Biology*, *20*(11), 4106–4114.

Kaur, C., Sivakumar, V., & Foulds, W. S. (2006). Early response of neurons and glial cells to hypoxia in the retina. *Investigative Ophthalmology & Visual Science*, *47*(3), 1126–1141. https://doi.org/10.1167/iovs.05-0518

Keren-Shaul, H., Spinrad, A., Weiner, A., Matcovitch-Natan, O., Dvir-Szternfeld, R., Ulland, T. K., … Amit, I. (2017). A unique microglia type associated with restricting development of Alzheimer's disease. *Cell*, *169*(7), 1276–1290 e1217. https://doi.org/10.1016/j.cell.2017.05.018

Kezic, J., Xu, H., Chinnery, H. R., Murphy, C. C., & McMenamin, P. G. (2008). Retinal microglia and uveal tract dendritic cells and macrophages are not CX3CR1 dependent in their recruitment and distribution in the young mouse eye. *Investigative Ophthalmology & Visual Science*, *49*(4), 1599–1608. https://doi.org/10.1167/iovs.07-0953

Kim, C. S., Shin, K. S., Lee, H. J., Jo, Y. J., & Kim, J. Y. (2014). Sectoral retinal nerve fiber layer thinning in branch retinal vein occlusion. *Retina*, *34*(3), 525–530. https://doi.org/10.1097/IAE.0b013e3182a2e746

Klein, R., Klein, B. E., Moss, S. E., & Meuer, S. M. (2000). The epidemiology of retinal vein occlusion: The beaver dam eye study. *Transactions of the American Ophthalmological Society*, *98*, 133–141.

Krasemann, S., Madore, C., Cialic, R., Baufeld, C., Calcagno, N., El Fatimy, R., … Butovsky, O. (2017). The TREM2-APOE pathway drives the transcriptional phenotype of dysfunctional microglia in neurodegenerative diseases. *Immunity*, *47*(3), 566–581 e569. https://doi.org/10.1016/j.immuni.2017.08.008

Kuno, R., Wang, J., Kawanokuchi, J., Takeuchi, H., Mizuno, T., & Suzumura, A. (2005). Autocrine activation of microglia by tumor necrosis factor-alpha. *Journal of Neuroimmunology*, *162*(1–2), 89–96. https://doi.org/10.1016/j.jneuroim.2005.01.015

Lambertsen, K. L., Meldgaard, M., Ladeby, R., & Finsen, B. (2005). A quantitative study of microglial-macrophage synthesis of tumor necrosis factor during acute and late focal cerebral ischemia in mice. *Journal of Cerebral Blood Flow and Metabolism*, *25*(1), 119–135. https://doi.org/10.1038/sj.jcbfm.9600014

Lim, R. R., Hainsworth, D. P., Mohan, R. R., & Chaurasia, S. S. (2019). Characterization of a functionally active primary microglial cell culture from the pig retina. *Experimental Eye Research*, *185*, 107670. https://doi.org/10.1016/j.exer.2019.05.010

Mantovani, A., Sica, A., Sozzani, S., Allavena, P., Vecchi, A., & Locati, M. (2004). The chemokine system in diverse forms of macrophage activation and polarization. *Trends in Immunology*, *25*(12), 677–686. https://doi.org/10.1016/j.it.2004.09.015

Mayhan, W. G. (1999). VEGF increases permeability of the blood-brain barrier via a nitric oxide synthase/cGMP-dependent pathway. *The American Journal of Physiology*, *276*(5 Pt 1), C1148–C1153.

Nadal-Nicolas, F. M., Jimenez-Lopez, M., Sobrado-Calvo, P., Nieto-Lopez, L., Canovas-Martinez, I., Salinas-Navarro, M., … Agudo, M. (2009). Brn3a as a marker of retinal ganglion cells: Qualitative and quantitative time course studies in naive and optic nerve-injured retinas. *Investigative Ophthalmology & Visual Science*, *50*(8), 3860–3868. https://doi.org/10.1167/iovs.08-3267

Nakazawa, T., Nakazawa, C., Matsubara, A., Noda, K., Hisatomi, T., She, H., … Benowitz, L. I. (2006). Tumor necrosis factor-alpha mediates oligodendrocyte death and delayed retinal ganglion cell loss in a mouse model of glaucoma. *The Journal of Neuroscience*, *26*(49), 12633–12641. https://doi.org/10.1523/jneurosci.2801-06.2006

Nandi, S., Gokhan, S., Dai, X. M., Wei, S., Enikolopov, G., Lin, H., … Stanley, E. R. (2012). The CSF-1 receptor ligands IL-34 and CSF-1 exhibit distinct developmental brain expression patterns and regulate neural progenitor cell maintenance and maturation. *Developmental Biology*, *367*(2), 100–113. https://doi.org/10.1016/j.ydbio.2012.03.026

Natoli, R., Fernando, N., Madigan, M., Chu-Tan, J. A., Valter, K., Provis, J., & Rutar, M. (2017). Microglia-derived IL-1beta promotes chemokine expression by Muller cells and RPE in focal retinal degeneration. *Molecular Neurodegeneration*, *12*(1), 31. https://doi.org/10.1186/s13024-017-0175-y

Noma, H., Mimura, T., & Eguchi, S. (2013). Association of inflammatory factors with macular edema in branch retinal vein occlusion. *JAMA Ophthalmology*, *131*(2), 160–165. https://doi.org/10.1001/2013.jamaophthalmol.228

Offner, H., Subramanian, S., Parker, S. M., Afentoulis, M. E., Vandenbark, A. A., & Hurn, P. D. (2006). Experimental stroke induces massive, rapid activation of the peripheral immune system. *Journal of Cerebral Blood Flow and Metabolism*, *26*(5), 654–665. https://doi.org/10.1038/sj.jcbfm.9600217

Paschalis, E. I., Lei, F., Zhou, C., Kapoulea, V., Dana, R., Chodosh, J., … Dohlman, C. H. (2018). Permanent neuroglial remodeling of the retina following infiltration of CSF1R inhibition-resistant peripheral monocytes. *Proceedings of the National Academy of Sciences of the United States of America*, *115*(48), E11359–E11368. https://doi.org/10.1073/pnas.1807123115

Patel, A. R., Ritzel, R., McCullough, L. D., & Liu, F. (2013). Microglia and ischemic stroke: A double-edged sword. *International Journal of Physiology, Pathophysiology and Pharmacology*, *5*(2), 73–90.

Patel, S., & Player, M. R. (2009). Colony-stimulating factor-1 receptor inhibitors for the treatment of cancer and inflammatory disease. *Current Topics in Medicinal Chemistry*, *9*(7), 599–610.

Pey, P., Pearce, R. K., Kalaitzakis, M. E., Griffin, W. S., & Gentleman, S. M. (2014). Phenotypic profile of alternative activation marker CD163 is different in Alzheimer's and Parkinson's disease. *Acta Neuropathologica Communications*, *2*, 21. https://doi.org/10.1186/2051-5960-2-21

Plane, J. M., Shen, Y., Pleasure, D. E., & Deng, W. (2010). Prospects for minocycline neuroprotection. *Archives of Neurology*, *67*(12), 1442–1448. https://doi.org/10.1001/archneurol.2010.191

Poon, C. C., Gordon, P. M. K., Liu, K., Yang, R., Sarkar, S., Mirzaei, R., … Kelly, J. J. P. (2019). Differential microglia and macrophage profiles in human IDH-mutant and -wild type glioblastoma. *Oncotarget*, *10*(33), 3129–3143. https://doi.org/10.18632/oncotarget.26863

Rivera, J. C., Sitaras, N., Noueihed, B., Hamel, D., Madaan, A., Zhou, T., … Chemtob, S. (2013). Microglia and interleukin-1beta in ischemic retinopathy elicit microvascular degeneration through neuronal semaphorin-3A. *Arteriosclerosis, Thrombosis, and Vascular Biology*, *33*(8), 1881–1891. https://doi.org/10.1161/atvbaha.113.301331

Rogers, S., McIntosh, R. L., Cheung, N., Lim, L., Wang, J. J., Mitchell, P., … International Eye Disease, C. (2010). The prevalence of retinal vein occlusion: Pooled data from population studies from the United States, Europe, Asia, and Australia. *Ophthalmology*, *117*(2), 313–319 e311. https://doi.org/10.1016/j.ophtha.2009.07.017

Roh, M., Zhang, Y., Murakami, Y., Thanos, A., Lee, S. C., Vavvas, D. G., … Miller, J. W. (2012). Etanercept, a widely used inhibitor of tumor necrosis factor-alpha (TNF-alpha), prevents retinal ganglion cell loss in a rat model of glaucoma. *PLoS One*, *7*(7), e40065. https://doi.org/10.1371/journal.pone.0040065

Ronning, K. E., Karlen, S. J., Miller, E. B., & Burns, M. E. (2019). Molecular profiling of resident and infiltrating mononuclear phagocytes during rapid adult retinal degeneration using single-cell RNA sequencing. *Scientific Reports*, *9*(1), 4858. https://doi.org/10.1038/s41598-019-41141-0

Sappington, R. M., Chan, M., & Calkins, D. J. (2006). Interleukin-6 protects retinal ganglion cells from pressure-induced death. *Investigative Ophthalmology & Visual Science*, *47*(7), 2932–2942. https://doi.org/10.1167/iovs.05-1407

Shichita, T., Sugiyama, Y., Ooboshi, H., Sugimori, H., Nakagawa, R., Takada, I., … Yoshimura, A. (2009). Pivotal role of cerebral interleukin-17-producing gammadeltaT cells in the delayed phase of ischemic brain injury. *Nature Medicine*, *15*(8), 946–950. https://doi.org/10.1038/nm.1999

Spangenberg, E. E., Lee, R. J., Najafi, A. R., Rice, R. A., Elmore, M. R., Blurton-Jones, M., … Green, K. N. (2016). Eliminating microglia in Alzheimer's mice prevents neuronal loss without modulating amyloid-beta pathology. *Brain*, *139*(Pt 4), 1265–1281. https://doi.org/10.1093/brain/aww016

Stirling, D. P., Koochesfahani, K. M., Steeves, J. D., & Tetzlaff, W. (2005). Minocycline as a neuroprotective agent. *The Neuroscientist*, *11*(4), 308–322. https://doi.org/10.1177/1073858405275175

Sun, C., Li, X. X., He, X. J., Zhang, Q., & Tao, Y. (2013). Neuroprotective effect of minocycline in a rat model of branch retinal vein occlusion. *Experimental Eye Research*, *113*, 105–116. https://doi.org/10.1016/j.exer.2013.05.018

Takeda, A., Shinozaki, Y., Kashiwagi, K., Ohno, N., Eto, K., Wake, H., … Koizumi, S. (2018). Microglia mediate non-cell-autonomous cell death of retinal ganglion cells. *Glia*, *66*(11), 2366–2384. https://doi.org/10.1002/glia.23475

Unger, M. S., Schernthaner, P., Marschallinger, J., Mrowetz, H., & Aigner, L. (2018). Microglia prevent peripheral immune cell invasion and promote an anti-inflammatory environment in the brain of APP-PS1 transgenic mice. *Journal of Neuroinflammation*, *15*(1), 274. https://doi.org/10.1186/s12974-018-1304-4

Vogel, D. Y., Vereyken, E. J., Glim, J. E., Heijnen, P. D., Moeton, M., van der Valk, P., … Dijkstra, C. D. (2013). Macrophages in inflammatory multiple sclerosis lesions have an intermediate activation status. *Journal of Neuroinflammation*, *10*, 35. https://doi.org/10.1186/1742-2094-10-35

Wang, Q., Tang, X. N., & Yenari, M. A. (2007). The inflammatory response in stroke. *Journal of Neuroimmunology*, *184*(1–2), 53–68. https://doi.org/10.1016/j.jneuroim.2006.11.014

Welser-Alves, J. V., & Milner, R. (2013). Microglia are the major source of TNF-alpha and TGF-beta1 in postnatal glial cultures; regulation by cytokines, lipopolysaccharide, and vitronectin. *Neurochemistry International*, *63*(1), 47–53. https://doi.org/10.1016/j.neuint.2013.04.007

Zhang, H., Sonoda, K. H., Qiao, H., Oshima, T., Hisatomi, T., & Ishibashi, T. (2007). Development of a new mouse model of branch retinal vein occlusion and retinal neovascularization. *Japanese Journal of Ophthalmology*, *51*(4), 251–257. https://doi.org/10.1007/s10384-007-0445-2

Zhou, T., Huang, Z., Sun, X., Zhu, X., Zhou, L., Li, M., … He, C. (2017). Microglia polarization with M1/M2 phenotype changes in rd1 mouse model of retinal degeneration. *Frontiers in Neuroanatomy*, *11*, 77. https://doi.org/10.3389/fnana.2017.00077

SUPPORTING INFORMATION

Additional supporting information may be found online in the Supporting Information section at the end of this article.

How to cite this article: Jovanovic J, Liu X, Kokona D, Zinkernagel MS, Ebneter A. Inhibition of inflammatory cells delays retinal degeneration in experimental retinal vein occlusion in mice. *Glia*. 2019;1–15. https://doi.org/10.1002/glia.23739